Journal of Biomolecular NMR (2005) 33: 63–68
DOI 10.1007/s10858-005-1281-7

NMR structure note

Refinement of the solution structure of rat Olfactory Marker Protein (OMP)

Nathan T. Wright[a], Joyce W. Margolis[b], Frank L. Margolis[b] & David J. Weber[a,*]
[a]*Department of Biochemistry and Molecular Biology, University of Maryland School of Medicine, 108 N. Greene St., Baltimore, Maryland, 21201;* [b]*Department of Anatomy and Neurobiology, University of Maryland School of Medicine, 20 Penn St., Baltimore, Maryland, 21201*

Received 26 May 2005; Accepted 15 July 2005

Key words: beta-clamshell fold, NMR, olfaction, olfactory marker protein, residual dipolar coupling

Biological context

Olfaction is important in many facets of animal survival, including reproductive/maternal functions, emotional responses, recognition of predators, and food selection. In a well-conserved mechanism among vertebrates, odorants are detected and then transduced into electrical signals by olfactory receptor neurons (ORNs). These signals are then transmitted to output neurons, which in turn relay the information to higher order olfactory centers. Olfactory marker protein (OMP) is expressed almost exclusively in mature olfactory receptor neurons and has thus been used as a marker for recognizing this cell type (Margolis, 1980; Buiakova et al., 1994). OMP is an abundant 19 kDa protein whose expression in these neurons is developmentally regulated and whose sequence is phylogenetically conserved in all vertebrates from fish to humans (Margolis, 1980). OMP knockout mice have provided insights into the function of this protein. Electro-olfactograms (EOGs) of the neuroepithelium of these mice show slower response and recovery times (Buiakova et al., 1996). Physiologically, the mice demonstrate a much higher odor detection threshold and poorer odor quality perception (Youngentob et al., 2001). Infection of these mice with an OMP-containing adenoviral vector rescues the wild-type phenotype, arguing that indeed OMP is important in odor signaling (Ivic et al., 2000).

Although abundant evidence suggests that OMP contributes to olfactory sensitivity, very little biochemical evidence exists to explain why this is so. OMP is neither glycosylated nor phosphorylated and shows no endogenous enzymatic activity. Additionally, it contains no obvious structural motifs, such as zinc or calcium binding domains. To begin to address the question of how the structure of OMP might influence its function inside a neuron, structures of rat OMP, determined by multi-dimensional NMR spectroscopy, and the structure of mouse OMP by X-ray crystallography at 2.3 Å resolution have been reported (Baldisseri et al., 2002; Smith et al., 2002). The superposition of the two structures indicates a very similar β-clamshell fold with an RMSD of 2.13 Å for the C^{α} atoms of residues in the β-sheets. Although the core of the protein is similar for the two structures, a 16-residue helix (helix 1) shows a different orientation between them. However, only a very few weak long-range NOE constraints orient this region in the NMR structure. Thus, the orientation of helix 1 is relatively undefined in this original structure (Baldisseri et al., 2002). In order to determine more precisely the orientation of helix 1 in solution, residual dipolar coupling values are now included in the refined NMR structure of OMP, which is described here.

*To whom correspondence should be addressed. E-mail: dweber@umaryland.edu

Materials and methods

Sample preparation

^{15}N labeled recombinant rat OMP was generated and purified as described previously (Carr et al., 1998; Baldisseri et al., 2000). NMR samples contained rat OMP (0.5–1.8 mM) in 10 mM Na_2HPO_4, 0.1 mM Na_4EDTA, 0.3 mM NaN_3 at pH 6.6 in 10% D_2O. All solutions used to prepare the NMR sample were filter-sterilized (0.2 μm pore size) and deoxygenated by purging with helium for 10 min.

For aligned samples, necessary to collect residual dipolar coupling data, OMP was prepared in radially compressed (stretched) polyacrylamide gels as previously described (Chou et al., 2001, 2002). Briefly, polyacrylamide gels were prepared to a final polyacrylamide concentration of 5.5% and cast in a gel stretcher apparatus with a 6 mm diameter (New Era Enterprises, Inc.) (Chou et al., 2001). After the gel polymerized, it was washed in doubly distilled deionized water for 1 h (×3) and soaked in the NMR buffer described above without OMP. The gel was then cut to 10 mm and soaked overnight in 400 μl of 0.6 mM OMP in the above NMR buffer, plus 20% D_2O and 0.4 mM sodium azide. The next day, the gel was placed into a stretching apparatus and forced through a funnel into an opened ended 5 mm diameter NMR tube. This results in stretching the gel from 10 to 20 mm in length by radial compression. The bottom of the tube was sealed with a plug, and a plunger was gently lowered on top of the gel. The plunger was sealed with parafilm prior to data collection.

Nuclear magnetic resonance

NMR spectra were collected at 37 °C with a Bruker DMX600 NMR spectrometer (600.13 MHz for protons) and a Bruker AVANCE 800 NMR spectrometer (800.27 MHz for protons) equipped with four frequency channels and a triple-resonance *z*-axis gradient 5 mm cryoprobe. Some of the data used in the structure calculations (Baldisseri et al., 2002) were collected with conventional triple resonance 3-axis gradient probes prior to the installation of the cryoprobes. For all experiments, the ^{1}H carrier was set on the water frequency and the ^{15}N carrier frequency was at 118.6 ppm. Water-flip-back and field gradient pulses were used to suppress the water signal without saturation. The data were processed on Linux Red Hat 9.0 with the software package NmrPipe (Delaglio et al., 1995). All proton chemical shifts are reported with respect to the H_2O or HDO signal, which is taken as 4.658 ppm downfield from external TSP (0.00 ppm) at 37 °C. A 2D IPAP ^{1}H–^{15}N HSQC was also collected on isotopic and aligned OMP samples as previously described (Ottiger et al., 1998). These data were separated into complementary in-phase and anti-phase matrices, each with $2048^* \times 512^*$ points in t_1 and t_2, and with acquisition times of 80.9 ms (^{15}N) and 122.1 ms (^{1}H). The processed matrices contained 4096 × 1024 real points F1 and F2. In the final processed data, the peak positions were determined using the contour averaging method with the data analysis program PIPP (Garrett et al., 1991).

Structure calculations

Inter-proton distances were derived from NOE cross-peaks and classified into five levels including strong, medium, medium-weak, weak, and very weak. NOEs were then assigned distance constraints with a lower limit of 1.8 Å and an upper limit of 2.9, 3.5, 4.2, 5, and 6 Å, respectively (Clore et al., 1986). Pseudoatom corrections were applied to the upper limit for degenerate methyl, methylene and aromatic ring protons, and restraints for methyl protons were shifted down one category. Only structurally useful constraints were used; therefore NOE correlations between geminal protons and vicinal methylene protons were excluded. Eighty residual dipolar couplings (in Hz) were determined from differences in *J* splitting between the isotropic and aligned phases of the 2D IPAP-HSQC data. The axial ($\mathbf{A_a} = 1.5 \times 10^{-3}$) and rhombic ($\mathbf{A_r} = 1.1 \times 10^{-3}$) components of the alignment tensor **A** were obtained from the residual dipolar coupling data histogram as previously described (Clore et al., 1998). The force constants for the residual dipolar coupling energies were slowly increased in concert with the force constants of the NOE energy during the cooling stage of the structure calculations. The initial force constants were small (0.001 kcal Hz^{-2}), and the final force constants were determined for the $^1D_{NH}$ residual dipolar couplings such that the calculated

structures represented the uncertainty in the actual residual dipolar coupling data sets (Drohat et al., 1999), which were collected twice under identical conditions.

Structures were calculated using XPLOR-NIH version 2.9.3, running on Linux using standard protocols for substructure embedding and regularization, hybrid distance geometry-simulated annealing (DGSA) regularization and refinement, and simulated annealing (SA) refinement (Schwieters et al., 2003). A conformational database potential and pseudo-potentials for secondary $^{13}C^{\alpha}$ and $^{13}C^{\beta}$ chemical shifts were included in the SA refinement. The refinement yielded many (>40) structures with no distance violations >0.4 Å or dihedral angle violations >5 degrees. PROCHECK was used to analyze the quality of the structures. Experimental residual dipolar coupling data were compared to dipolar coupling values back-calculated from the final structures using the program PALES, and such comparisons were used for Q-factor calculations (Zweckstetter et al., 2004). In this regard, the Q-factor was calculated by randomly leaving out 10% of the $^{1}D_{NH}$ data in 6 different trials and taking the average Q-value from the separate calculations.

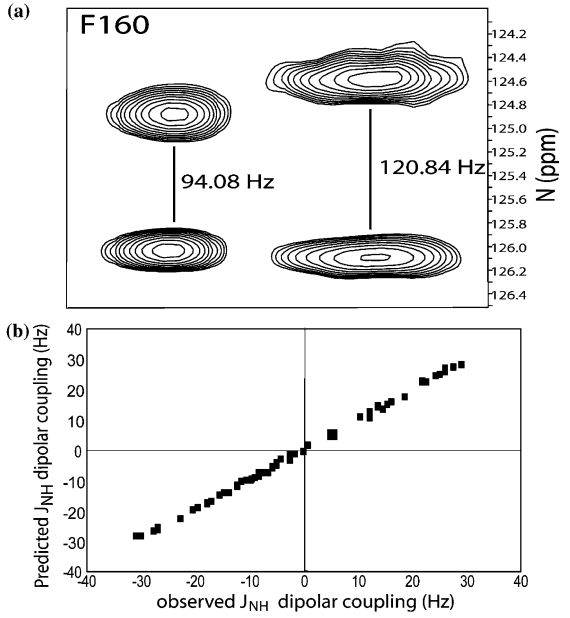

Figure 1. Representative 2D IPAP-HSQC data used to measure residual dipolar couplings for OMP. (a) A small region of the 2D ^{1}H–^{15}N HSQC illustrating splitting of residue Phe-160. The residual dipolar couplings were determined by comparing ^{1}H–^{15}N splitting recorded in the presence (right) or absence (left) of compressed 5% acrylamide gel media. (b) The correlation between the observed backbone NH residual dipolar couplings and the predicted residual dipolar couplings of the lowest energy structure is illustrated.

Results and discussion

IPAP-HSQC experiments were run on isotropic and aligned samples of ^{15}N-labeled OMP. A total of 80 $^{1}D_{NH}$ residual dipolar couplings (RDCs) ranging from −31 to 26 Hz (Figure 1a) were measured in order to reconcile the disparity regarding the position of helix 1 in the X-ray and NMR structures of OMP (Baldisseri et al., 2002; Smith et al., 2002). Data from separate samples, prepared under identical conditions and using the same gel compression technique, were in quite good agreement (RMSD = 0.46 Hz). The $^{1}D_{NH}$ residual dipolar couplings were found to fit reasonably well to the X-ray structure (Q-factor = 0.28) but very poorly to the original NOE-based NMR structure (Q = 0.72) (Baldisseri et al., 2002; Smith et al., 2002).

The high Q-factor of the original NMR structure was due primarily to the orientation of the poorly defined helix 1, which has very few NOE constraints (Baldisseri et al., 2002; Smith et al., 2002). Specifically, only 8 long-range NOE correlations were observed from residues in helix 1 (residues L21, M25, and V29) to loop 1 (residue L45, L46) and/or to the second β-strand (V52). The incorporation of the $^{1}D_{NH}$ residual dipolar coupling constraints into the structure calculation was found to extend this helix away from the β-clam region of the protein as found previously in the X-ray structure (Figures 2 and 3), and the resulting quality factor of the NMR structure was dramatically improved ($Q = 0.21 \pm 0.06$). Consequentially, residues in the C-terminal portion of the helix are quite distant from most residues in the protein, thus explaining why the position of this helix was not accurately defined using NOE correlations alone.

In total, the refined solution NMR structure of OMP was determined using 1764 constraints (10.8 per residue; Table 1). This included 271 intra-residue, 511 sequential, 242 medium range, 319 long-range, 124 hydrogen bonds, 217 dihedral restraints

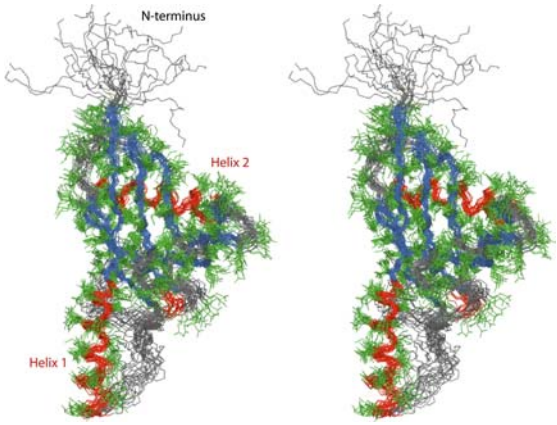

Figure 2. Overlay of the 20 best NMR structures of OMP in stereo view. Residues in β-strands are colored in blue, helical regions are colored in red, and random coil regions are colored in gray. Sidechains for ordered residues in OMP (Q9-R35, E50-T83, A103-L163) are colored in green.

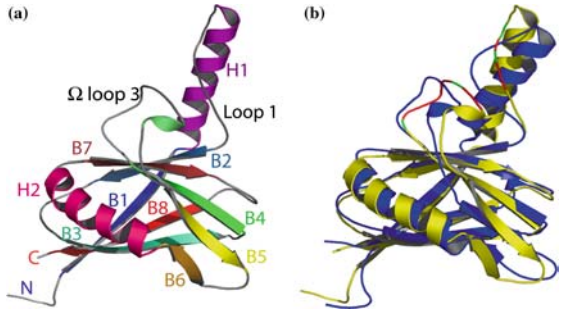

Figure 3. Comparison of the refined NMR structure and X-ray structure of OMP. (a) A ribbon diagram of the lowest energy structure of OMP. Helix 1 is colored purple and helix 2 is colored pink in this representation. (b) Superposition of the lowest energy NMR structure (yellow) with that of the X-ray structure (blue). The RMSD of the backbone atoms of well-ordered residues between these two structures is 1.61. Residues Asp-41 to Ala-49 and Phe-84 to Thr-96 are dynamic regions in OMP and are colored red on the lowest energy NMR structure. Residues in these two loops that lacked NMR constraints are colored green (loop 1: K39, Q40, G42; Ω-loop 3: Q85, N93).

(Φ and Ψ angles), and 80 $^{1}D_{NH}$ dipolar coupling constraints. Importantly, nine residual dipolar coupling constraints (from 16 possible) were measured for residues in helix 1. The 20 lowest energy structures had no NOE violations (>0.4 Å) or dihedral violations (>5 degrees), and the majority of residues were located in the most favorable regions of the Ramachandran diagram (87.0%) with none in the disallowed region (Table 1). The ensemble of these 20 structures has low deviations from experimental constraints and has an RMSD $= 1.355 \pm 0.196$ for all heavy atoms and an RMSD $= 0.640 \pm 0.081$ for backbone residues in the ordered regions of OMP (Table 1); and the RMSD for the experimental residual dipolar couplings is 0.49 ± 0.03 Hz. The NMR structural data and the coordinates for these 20 lowest structures are deposited in the Protein Data Bank (PDB code: 1ZRI).

The secondary structure of OMP in the refined solution structure is similar, but not identical, to that previously reported (Baldisseri et al., 2000; Smith et al., 2002). Specifically, OMP has two long α-helices and eight β-strands including β1 (Q9-D18), α1 (Q19-Q34), β2 (E50-D56), β3 (L63-D73), β4 (G76-T83), β5 (A104-K109), β6 (M115-N118), α2 (E119-K134), β7 (V138-T144), and β8 (L154-Q162). Additionally, a small alpha-helical region, Thr-96 to Gln-98, was observed based on the analysis of the 3D NMR structure. This small region is also present in the X-ray structure of murine OMP.

The overall fold of the newly refined OMP structure also shares many similarities with the earlier published structures (Baldisseri et al., 2002; Smith et al., 2002). OMP is a single globular domain protein comprised of two β-sheets oriented orthogonally to one another in a β-clamshell fold (Figures 2 and 3). Several of the beta strands, most notably β7, have a significant twist to them. In the case of β7, this orientation functions to accommodate hydrogen bonding to both β-sheets, with interactions with β4 in the first sheet and β2 in the second sheet. Thus the β-strands, though arranged in a sandwich-like conformation, display an undisrupted network of hydrogen bonding (Figure 3a). On opposite sides of the β-clamshell domain there are two long helices (helices 1 and 2), which are perpendicularly oriented. There are also three large extended loop regions of OMP including loop 1 (residues G36-A49), loop 2 (residues F57-L63), Ω loop 3 (residues S84-A103); the Ω loop is homologous to the EphB2-receptor, and may thus be important for regulating protein–protein interactions.

When the refined NMR and X-ray structures of OMP are superimposed, the interhelical angle between helices 1 and 2 for the ensemble of NMR structures is slightly more closed ($88 \pm 4°$) than in the X-ray crystal structure (100°) (Figure 3b).

Table 1. NMR-derived restraints and statistics of 20 NMR structures[a]

	<20>	Best
RMSD from distance constraints (Å)[b]		
Total (1467)	0.035 ± 0.002	0.032
Intraresidue (271)	0.000 ± 0.000	0.000
Sequential (| *i*–*j*| = 1) (511)	0.031 ± 0.004	0.028
Medium-range (1 < | *i*–*j*| ≤ 1) (242)	0.034 ± 0.005	0.035
Long-range (| *i*–*j*| > 5) (319)	0.039 ± 0.004	0.030
Hydrogen bonds (124)	0.068 ± 0.005	0.062
RMSD from exptl dihedral constraints (°)		
Φ, Ψ (217)	0.664 ± 0.075	0.667
RMSD from dipolar coupling restraints (Hz)		
$^{1}D_{NH}$ (80)	0.485 ± 0.032	0.482
RMSD from exptl ^{13}C chemical shifts		
$^{13}C\alpha$ (ppm)	1.255 ± 0.061	1.390
$^{13}C\beta$ (ppm)	2.657 ± 0.809	2.732
RMSD from idealized geometry		
Bonds (Å)	0.004 ± 0.000	0.004
Angles (°)	0.546 ± 0.022	0.568
Impropers (°)	0.496 ± 0.021	0.504
Lennard–Jones potential energy (kcal mol^{-1})[c]	−606 ± 19	−604
Region of the Ramachandran plot[d]		
Most favorable	87.0 ± 2.1	89.0
Additionally allowed	11.1 ± 2.4	8.9
Generously allowed	1.9 ± 0.8	2.1
Dissallowed	0.0 ± 0.0	0
RMSD to the mean structure (Å)[e]		
Ordered backbone	0.640 ± 0.081	0.546
Ordered heavy atoms	1.355 ± 0.106	1.235

[a]The 20 ensemble structures, <20>, are the results of simulated annealing calculations. The best structure is chosen from the lowest total energy. The values shown for the <20> are the mean ± standard deviation.
[b]None of the 20 structures has a distance violation > 0.4 Å or a dihedral angle violation of >5°. The force constants used in the SA calculations are as follows: 1000 kcal mol^{-1} Å^{2} for bond length, 500 kcal mol^{-1} rad^{-2} for angles and improper torsions, 4 kcal mol^{-1} Å^{-4} for the quartic van der Waals (vdw) repulsion term (hard-sphere effective vdw set to 0.8 times their values in CHARMm parameters), 50 kcal mol^{-1} Å^{-2} for experimental distance constraints, 100 kcal mol^{-1} Å^{-2} for non-crystallographic symmetry, 1 kcal mol^{-1} Å^{-2} for distance symmetry constraints, 0.5 kcal mol^{-1} ppm^{-2} for the ^{13}C chemical shift constraints, and 1.0 for the conformational database potential. The force constant (in kcal Hz^{-2}) used for residual dipolar coupling restraints was 1.30 for ^{15}N–$^{1}H^{N}$.
[c]Lennard–Jones van der Waals energies were calculated using CHARMm parameters and were not used in any stage of the structure determination.
[d]PROCHECK was utilized to generate the Ramachandran plot.
[e]Backbone calculations include C^{α}, N, and C′ atoms. Ordered backbone residues consist of 11–34, 50–83, and 103–163, as these are the residues that contain either long range interactions or regular secondary structure motifs.

Another area of decreased overlap between the NMR and X-ray structures is the positioning of loop 3 (residues S84-A103) and loop 1 (residues G35-A49). In the X-ray structure, loops 1 and 3 are aligned in a parallel manner with numerous protons from residues Gly-42 to Lys-44 of loop 1 and residues Asn-93 to Met-95 being proximal (<4 Å); in the NMR structure, only 1 very weak NOE could be found between these loop residues (from K44 to L94) even when looking deep into the noise of the NOESY data. The lack of NOE correlations in these regions is likely due to the dynamic properties of OMP (Gitti et al., 2005), which must be suppressed upon crystallization.

Specifically, residues that exhibit exchange broadening ($R_{ex} > 1$/sec) are located in helix 1 (D20-K33), loop 1 (R35, G42-A49), Ω-loop 3 (S84-T96, N98-L99), and in the N- and C-termini. Likewise, fast timescale motions (τ_e) and low order parameters ($S^2 < 0.7$) occur in loop 1 (K39, Q40), and resonances for Gly-42 are missing altogether in OMP spectra. Therefore it is possible that this small region in loop 1 (K39-G42) serves as a hinge to allow for the dynamics observed in these two loops and helix 1 and can explain the differences observed between the NMR and X-ray structures. In summary, the only region of OMP that was not adequately defined by our NMR data was this small highly dynamic region in loop 1 (K39, Q40, G42) and Ω-loop 3 (Q85, N93) and a few other residues scattered throughout the protein (Q61, L72, T79); otherwise, the NMR data was sufficient to accurately define the position of helix 1 and all other residues of OMP.

Conclusion

In this study, the solution structure of Olfactory Marker Protein (OMP) was refined by NMR spectroscopy. This protein is a monomeric globular protein with its core made up of eight β-strands composing a β-clamshell domain. The secondary structure within this domain is well defined. The orientation of helix 1, which was previously only poorly defined using short-range NOE constraints, is now well-defined with the inclusion of long-range residual dipolar coupling constraints. The position of helix 1 is now very similar to that observed previously by X-ray crystallography, despite the fact that there exists some dynamic character in this helix and in loops 1 and 3 of OMP (Gitti et al., 2005).

Acknowledgements

This work was supported by grants from the National Institutes of Health (GM58888 to D.J.W.), and NIH-DC03112 (F.L.M.). N.T.W. was supported by an NIH training Grant T32-AR07592 from the Interdisciplinary Training Program in Muscle Biology, University of Maryland, Baltimore. This work also made use of the University of Maryland School of Medicine NMR facility, which is supported by several shared instrumentation grants from the NIH and the NSF.

References

Baldisseri, D.M., Margolis, J.W., Omotosho, P.A., Volkman, B.F. and Margolis, F.L. (2000) *J. Biomol. NMR*, **17**, 353–354.
Baldisseri, D.M., Margolis, J.W., Weber, D.J., Koo, J.H. and Margolis, F.L. (2002) *J. Mol. Biol.*, **319**, 823–837.
Buiakova, O.I., et al. (1996) *Proc. Natl. Acad. Sci. USA*, **93**, 9858–9863.
Buiakova, O.I., Krishna, N.S., Getchell, T.V. and Margolis, F.L. (1994) *Genomics*, **20**, 452–462.
Carr, V.M., Walters, E., Margolis, F.L. and Farbman, A.I. (1998) *J. Neurobiol.*, **34**, 377–390.
Chou, J.J., Gaemers, S., Howder, B., Louis, J.M. and Bax, A. (2001) *J. Biomol. NMR*, **21**, 377–382.
Chou, J.J., Kaufman, J.D., Stahl, S.J., Wingfield, P.T. and Bax, A. (2002) *J. Am. Chem. Soc.*, **124**, 2450–2451.
Clore, G.M., Brunger, A.T., Karplus, M. and Gronenborn, A.M. (1986) *J. Mol. Biol.*, **191**, 523–551.
Clore, G.M., Gronenborn, A.M. and Bax, A. (1998) *J. Magn. Reson.*, **133**, 216–221.
Delaglio, F., Grzesiek, S., Vuister, G.W., Zhu, G., Pfeifer, J. and Bax, A. (1995) *J. Biomol. NMR*, **6**, 277–293.
Drohat, A.C., Tjandra, N., Baldisseri, D.M. and Weber, D.J. (1999) *Protein Sci.*, **8**, 800–809.
Garrett, D.S., Powers, R., Gronenborn, A.M. and Clore, G.M. (1991) *J. Magn. Reson.*, **95**, 214–220.
Gitti, R., Wright, N.T., Margolis, J.W., Varney, K.M., Weber, D.J. and Margolis, F.L. (2005) *Biochemistry*, **44**, 9673–9679.
Ivic, L., Pyrski, M.M., Margolis, J.W., Richards, L.J., Firestein, S. and Margolis, F.L. (2000) *Nat. Neurosci.*, **3**, 1113–1120.
Margolis, F.L. (1980) In *Proteins of the Nervous System*, Bradshaw, R.A. and Scheider, D. (Eds.), Raven, New York, pp. 59–84.
Ottiger, M., Delaglio, F. and Bax, A. (1998) *J. Magn. Reson.*, **131**, 373–378.
Schwieters, C.D., Kuszewski, J.J., Tjandra, N. and Clore, G.M. (2003) *J. Magn. Reson.*, **160**, 65–73.
Smith, P.C., Firestein, S. and Hunt, J.F. (2002) *J. Mol. Biol.*, **319**, 807–821.
Youngentob, S.L., Margolis, F.L. and Youngentob, L.M. (2001) *Behav. Neurosci.*, **115**, 626–631.
Zweckstetter, M., Hummer, G. and Bax, A. (2004) *Biophys. J.*, **86**, 3444–3460.